



Source parameters estimation from gravity data using Bat algorithm with application to geothermal and volcanic activity studies

K. S. Essa¹ · Z. E. Diab¹

Received: 12 November 2021 / Revised: 8 April 2022 / Accepted: 1 May 2022 / Published online: 3 June 2022

© The Author(s) under exclusive licence to Iranian Society of Environmentalists (IRSEN) and Science and Research Branch, Islamic Azad University 2022

Abstract

Recently gravity data modeling plays an important role in the study of volcanic activity and geothermal investigation. Generally, gravity data modeling assumes the subsurface either homogenous or spatially variable densities within modeled source rocks and surrounding sediments. As a result, the subsurface geothermal and volcanic goals and targets are included and validated using simple-geometric sources in gravity data modeling. The Bat algorithm, which is considered one of the most recently, developed metaheuristic algorithms in geophysics applications, permits to discovery and delineation of the source's parameters. Here, we presented the contribution of the Bat algorithm technique in elucidating 2D gravity profiles for geothermal exploration and volcanic activity cases. The Bat algorithm is based on the echo-location behavior of bats to perform global optimization. The Bat optimization algorithm is applied to 2D gravity data to estimate the source's parameters such as depth, origin location, amplitude factor, and geometric shape of the causative buried body. The stability and efficiency of the introduced optimizing algorithm were checked to different synthetic cases, i.e., for model 1, which represents a horizontal cylinder model, and model 2 represents a multi-sources effect. Furthermore, the successful applications of the proposed algorithm for discovering the geothermal and volcanic activities in Japan and India were have presented. The obtained results are in good agreement with the available geological, geophysical, and borehole information.

Keywords Bat algorithm · Geothermal investigation · Gravity anomaly · Source depth · Volcanic activity

Introduction

Nowadays, gravity data was gathered in large quantities for environmental and geological applications, such as oil and mineral explorations, groundwater investigations, geothermal investigations, and volcanic activity studies. The accurate estimation of the depth to the body sources improves in budgeting and preparing drill boreholes and exploration programs. In the oil industry, for example, accurate assessments of basement depth are important for understanding the basin exploration (the thickness of the sedimentary layer) more clearly and reduce the exploration risk factor (Li and Oldenburg 1983; Florio 2020). Gravity data are needed for oil exploration mapping of sedimentary basins and salt

structures (Sarsar Naouali et al. 2017; Essa et al. 2021a). In mineral and ore exploration, the estimation of the dominant orebody parameters (depth, types, shape,...etc.) reduces the risk associated with mining and plan for future investments (Snowden et al. 2002; Sultan et al. 2009; Zhang et al. 2022). In engineering and environmental studies, the gravity method has important uses in exploring, locating, and distinguished the subsurface voids, karst, buried hazardous metal containers, mapping landfills, delineating abruptly dipping geologic contacts and disruptions, visualizing regions of potential stress amplifications such as faults (Hinze et al. 2013; Eshanibli et al. 2021). In geothermal exploration, the gravity data elucidation mainly purposes to assess the location and depth of the sources, which are crucial to targeting the geothermal potential reservoirs anomalies (Athens and Caers 2021). In volcanic activities studies, the gravity method can clarify the geodynamic process based on their temporal variations, which have got up from earthquakes and volcanic activity (Lichoro et al. 2019; Casallas-Moreno et al. 2021).

Editorial responsibility: Maryam Shabani.

✉ Z. E. Diab
zdiab@cu.edu.eg

¹ Department of Geophysics, Faculty of Science, Cairo University, Giza 12613, Egypt



Generally, the gravity method has been receiving attention in more targets as declared above because it can elucidate and visualize the variant anomaly structures. So, several methods for the complete interpretation were developed and categorized as follows: 1) Conventional and non-conventional methods, which depend on the characteristic distance and points, nomograms, matching curves, window and depth curves, various types of transformations, minimization algorithms, gradients-based, moving average, Euler deconvolution, DEXP, fair function minimization (Telford et al. 1990; Abdelrahman et al. 2003; Al-Garni 2008; Asfahani and Tlas 2012; Essa 2013; Abdelrahman and Essa 2015; Ekinici and Yiğitbaş 2015; Hiramatsu et al. 2019; Cooper 2021). 2) Methods depend on 2D and 3D imaging, modeling, and inversion (Zhang et al. 2001; Asfahani and Tlas 2015; Essa et al. 2020). 3) Methods used simple geometric shapes such as spheres, cylinders, faults, and contacts (Biswas 2015; Tlas and Asfahani 2018; Uzun et al. 2020; Essa 2021). 4) Methods rely on the application of the global optimization algorithms such as particle swarm optimization (PSO), differential evolution algorithms (DE), simulated-annealing (SA), genetic algorithms (GA), ant-colony optimization (AC), gravitational search algorithm (GSA) (Biswas 2016; Kaftan 2017; Pallero et al. 2017; Essa and Munsch 2019; Essa and Géraud 2020; Rathee and Chhillar 2020; Pace et al. 2021).

Bat algorithm represents one of the recent proposed metaheuristic algorithms simulating the echolocation attitude of bats to obtain global optimization in geophysics especially, a potential field. In recent decades, many metaheuristic inspiring algorithms have been developed to solve complex problems (Mirjalili et al. 2014). For example, the genetic algorithm (GA) (Holland 1984; Montesinos et al. 2005), the particle swarm optimization (PSO) algorithm (Kennedy and Eberhart 1995; Roshan and Singh 2017; Essa 2021; Essa et al. 2021b), the differential evolution (DE) algorithm (Storn and Price 1997; Ekinici et al. 2016), the simulated annealing (SA) algorithm (Kirkpatrick et al. 1983; Biswas 2015), the ant colony optimization (ACO) algorithm (Dorigo et al. 1996; Dorigo and Stützle 2003), bee colony algorithm (Karaboga and Basturk 2008) dolphin echolocation (Kaveh and Farhoudi 2013), and gravitational search algorithm (Rashedi 2009).

In comparison to traditional optimization techniques, these algorithms are common among researchers because of their versatility and superior ability to deal with a variety of problems. These swarm intelligence algorithms have been developed and applied to various real-world problems, but the use of the Bat algorithm in geophysical data analysis is relatively new (i.e., in seismic refraction; Poormirzaee 2017; Poormirzaee et al. 2019). Fister (2013) concluded that the Bat algorithm outperforms the PSO after conducting various experiments on the implementation of the Bat algorithm.

Although methods like genetic algorithms (GA) and PSO can be quite beneficial, they still have certain limitations when it comes to multi-modal optimization issues (Yang 2013).

The proposed Bat algorithm technique have several advantages: One of the key advantages of this technique is that it provides highly quick convergence by switching from exploration to exploitation at a reasonably early stage. This makes it a good choice for applications that require a quick response, such as classifications. Bat algorithm may be

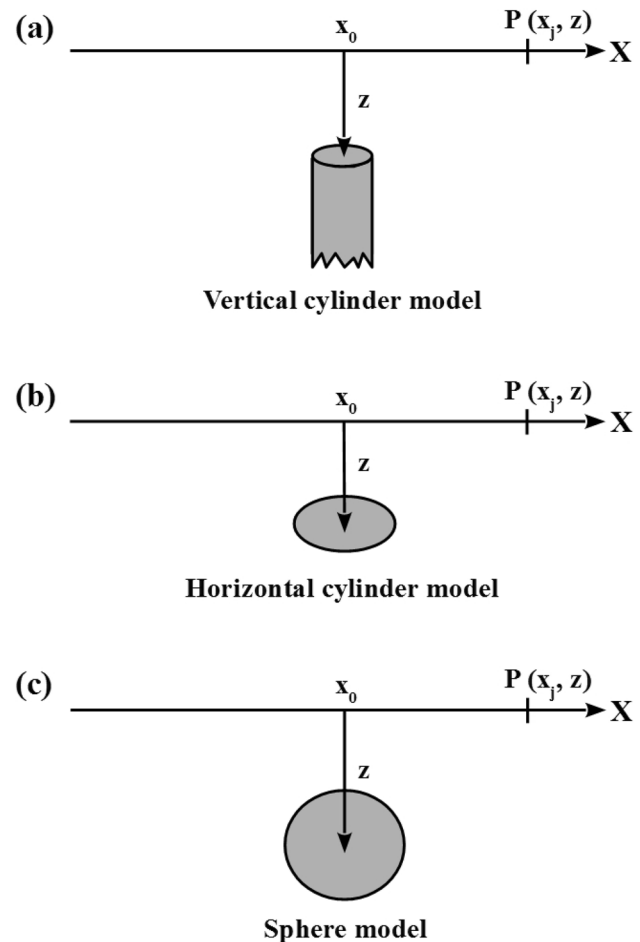


Fig. 1 The schematic diagrams for the different geometrical shapes

Table 1 Definitions of A , q and μ of the idealized bodies shown in Fig. 1. σ is the density contrast (gm/cm^3), γ is the universal gravitational constant ($6.67384 \times 10^{-11} \text{ m}^3 \text{ kg}^{-1} \text{ s}^{-2}$), and r is the radius of the idealized body (m)

Case	A	q	μ
Vertical cylinder	$\pi\gamma\sigma r^2$	$1/2$	0
Horizontal cylinder	$2\pi\gamma\sigma r^2$	1	1
Sphere	$\frac{4}{3}\pi\gamma\sigma r^3$	$3/2$	1

Fig. 2 Bat algorithm (BA) pseudo-code (modified after yang 2010)

```

Define Objective Function  $F_{Obj}(x_j)$  [equation (8)]
Initialize the bat population  $X_i$  ( $i = 1, 2, \dots, n$ ) and  $V_i$ 
Define pulse frequency  $Q_i$  at  $X_i$ 
Initialize pulse rates  $r_i$  and the loudness  $L_i$ 
while ( $t < \text{Max number of iterations}$ )
    Generate new solutions by adjusting frequency, and updating velocities
    and locations/solutions [equations (2) to (4)]
    if ( $rand > r_i$ )
        Select a solution among the best solutions Generate a local
        solution around the selected best solution
    end if
    Generate a new solution by flying randomly
    if ( $rand < L_i$  &  $F_{Obj}(X_i) < F_{Obj}(X_{best})$ )
        Accept the new solutions
        Increase  $r_i$  and reduce  $L_i$ 
    end if
    Rank the bats and find the current  $X_{best}$ 
end while

```

used as both a global and a local optimizer and is capable of effectively handling multi-model problems. As the iteration advances, Bat algorithm uses the controlling parameter to update the parameter. Bat algorithm is committed to preserving the population's diversity of solutions. The drawbacks of the Bat algorithm technique lie in the following items: It has a lack of good exploration. It required the parameter tuning to achieve better search output. Switching between exploration and exploitation requires a better control strategy.

Finally, the present study aims to infer and elucidate the 2D gravity data profile acquired over geothermal and volcanic areas in different regions in the world to estimate the source origin (depth & location) using the Bat algorithm technique, which is discussed below.

The structure of the paper organized as follows: “Bat algorithm” section covers the fundamentals of echolocation as well as the conventional formulation of the Bat algorithm. The “Forward modeling” section describes the modeling and formulation of the proposed Bat algorithm. The “Methodology” section provides the methodology of the proposed Bat algorithm to invert gravity data. The “Synthetic datasets”

section discusses the synthetic dataset examples accuracy and efficiency. The “Field datasets” section discusses the applicability of the proposed Bat algorithm to various field data examples. Finally, “Conclusions” section is drawn.

Bat algorithm

Bat algorithm (BA), which is a natural-inspired metaheuristic algorithm, was introduced by Yang (2010). The echolocation actions of micro-bats inspired this algorithm. Micro-bats use echolocation to locate their nest in the dark, avoid obstacles, and track prey. Bats release a very noisy sound pulse within 8 to 10 kHz in range and then listening to an echo backing from nearby objects. Every pulse is a few thousandths of a second long (up to about 8 to 10 ms). When bats are close to prey or an object, their pulses rate increases while their sound volume decreases (Yang 2010). As a result, the echolocation activity of micro-bats can be expressed in a way to optimize objective functions. The main rules of the Bat algorithm can shorten in three stages: first, Bats are applying the echolocation to assess distance;



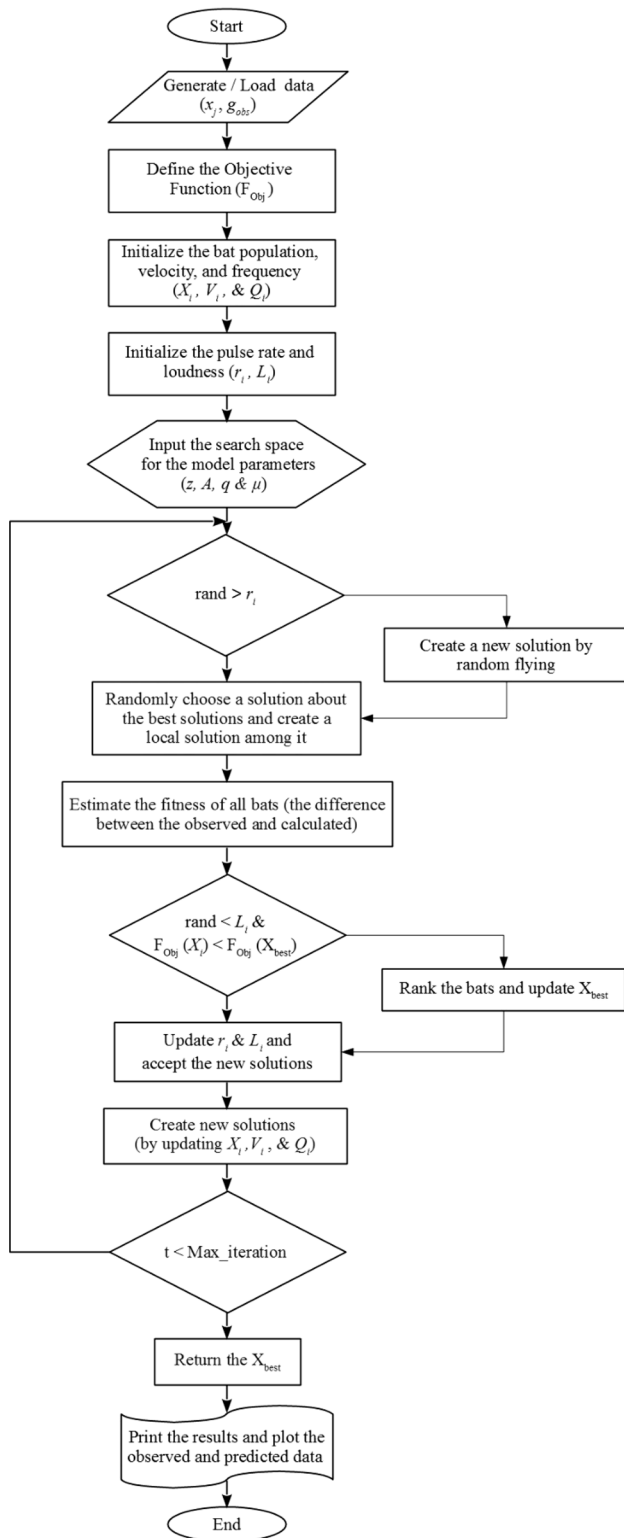


Fig. 3 The flowchart shows the public steps of The Bat algorithm (BA)

second, Bats are locating their sources objects by flying at a stable frequency in a range of $[Q_{\min}, Q_{\max}]$ with an initial speed (V_i) at position (X_i); and third, the loudness (L_i) and rate of pulse emission (r_i) which depend on the distance between the bat and the source.

The wavelength spectrum $[K_{\min}, K_{\max}]$ refers to the frequency range $[Q_{\min}, Q_{\max}]$. For an optimization problem, changing the frequency or wavelength may be used to change the movement range of bats (Eqs. 1–3). The selection of a suitable frequency or wavelength range is critical, and it should select to be equal to the scale of the domain of awareness before toning down to smaller ranges. The spectrum of $[0, 0.5]$ was calculated as the optimal frequency range in this analysis after the code runs with various values. The pulse rate, r_i , can be simply in the range $[0, 1]$, which 0 denotes no pulse and 1 is the maximum pulse emission rate. The range is determined by the target's proximity. Moreover, the initial loudness, i.e., L_i , can be normally within the range $[1, 2]$ (Yang 2010). The loudness of the bats decreases as they approach their prey, whereas the rate of pulse emission increases. Only if the new solutions improve can the Bat algorithm update the loudness and emission rates, indicating that the bats are approaching the optimal solution (Fister 2013; Eqs. 4–5). The equations below presented the relationship between algorithm parameters (Yang 2010).

$$Q_i^t = Q_{\min} + (Q_{\max} - Q_{\min})\beta \quad (1)$$

$$V_i^{(t+1)} = V_i^t + (X_i^t - X_{\text{best}})Q_i^t \quad (2)$$

$$X_i^{(t+1)} = X_i^t + V_i^{(t+1)} \quad (3)$$

$$L_i^{(t+1)} = \alpha L_i^t \quad (4)$$

$$r_i^t = r_i^0 [1 - \exp(-\gamma \tau)] \quad (5)$$

where, Q_i is the frequency of i^{th} bat and updated in every iteration, β is a random vector of uniform distribution within a range $[0, 1]$ and X_{best} is currently the global best solution among all bat numbers, α and γ are constants, $0 < \alpha < 1$ and $\gamma > 0$ and τ is the scaling factor.

Fig. 4 Model 1: noise-free theoretical example. **a** The observed gravity anomaly generated by horizontal cylinder model (True model parameters), as well as the calculated gravity anomaly (Recovered model parameters) using the Bat algorithm technique, **b** loudness of the bats, **c** emission rate of the bats, **d** NRMSE of the global best solution (F_{Obj}) of the bats versus the iteration numbers, and **e** the average NRMSE of all the bats

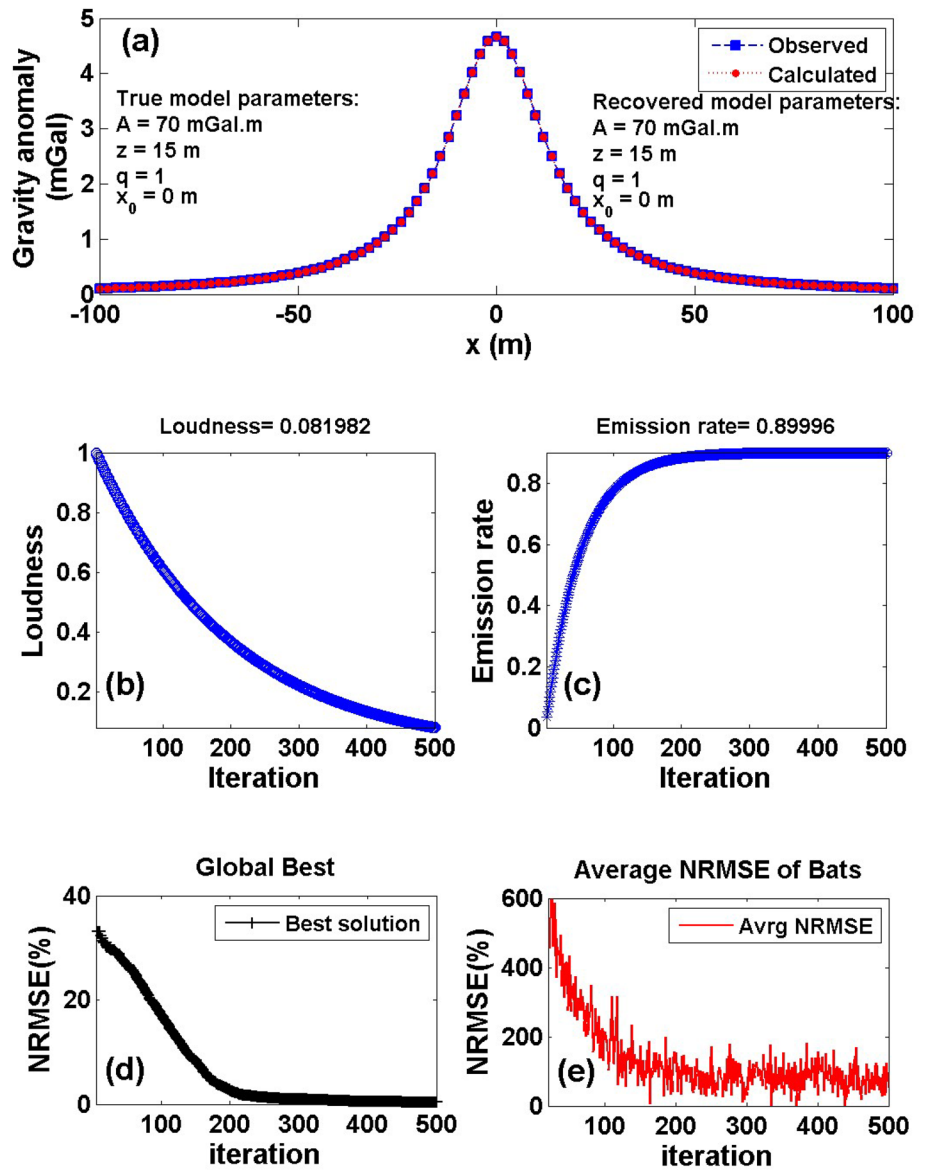


Table 2 Model-1: True and recovered model parameters of the noise-free synthetic example with corresponding RE and SD for each parameter using the Bat algorithm

Model parameters	True value	Search range	Recovered value	RE (%)	SD	OF_{Obj}
A (mGal.m)	70	10: 100	70	0	30.27	0.0000
z (m)	15	1: 20	15	0	5.91	
x_0 (m)	0	- 100: 100	0	0	58.60	
q	1	0.5: 1.5	1	0	0.50	
μ	1	0: 1	1	0	0.70	

Fig. 5 Model 1: Noisy theoretical example. **a** The observed gravity anomaly generated by horizontal cylinder model (True model parameters) after added 20% random Gaussian noise, as well as the calculated gravity anomaly (Recovered model parameters) using Bat algorithm technique, **b** loudness of the bats, **c** emission rate of the bats, **d** NRMSE of the global best solution (F_{Obj}) of the bats versus the iteration numbers, and **e** the average NRMSE of all the bats

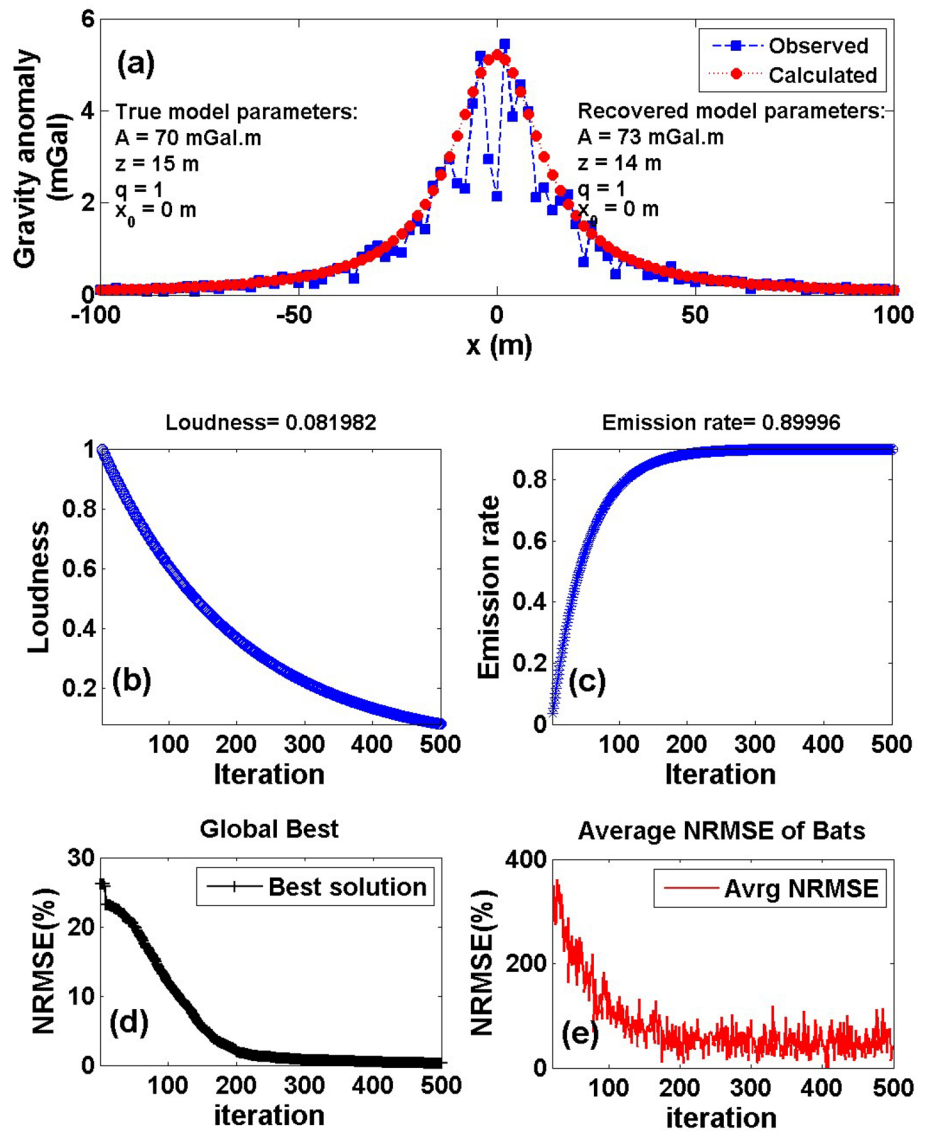
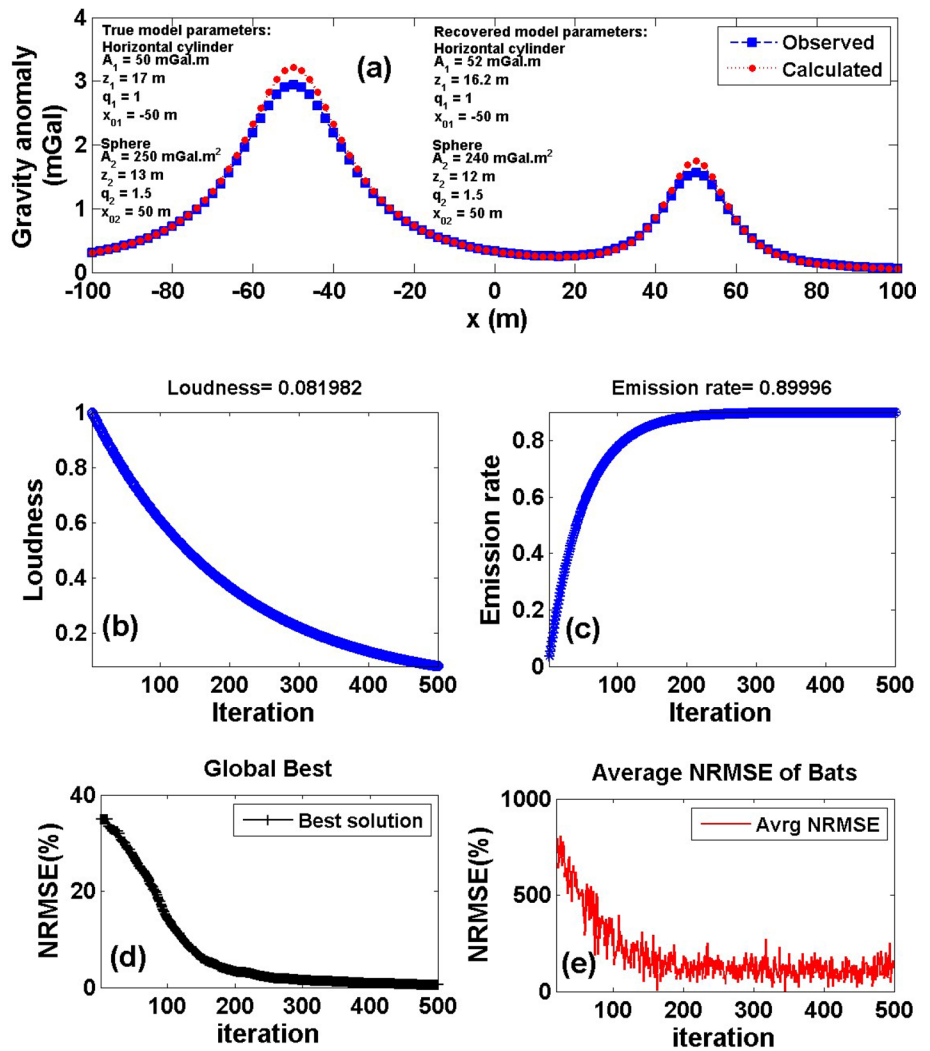


Table 3 Model-1: True and recovered model parameters of the noisy synthetic example (20% random Gaussian noise) with corresponding RE and SD for each parameters using the Bat algorithm

Model parameters	True value	Search range	Recovered value	RE (%)	SD	OF _{Obj}
A (mGal.m)	70	10: 100	73	4.28	26.41	0.0009
z (m)	15	1: 20	14	6.66	6.05	
x_0 (m)	0	- 100: 100	0	0	58.60	
q	1	0.5: 1.5	1	0	0.50	
μ	1	0: 1	1	0	0.70	

Fig. 6 Model-2: Interference effect. **a** The composite gravity anomaly generated by horizontal cylinder and sphere model (True model parameters), as well as the calculated gravity response of them (Recovered model parameters) using the Bat algorithm technique, **b** loudness of the bats, **c** emission rat of the bats, **d** NRMSE of the global best solution (F_{Obj}) of the bats versus the iteration numbers, and (e) the average NRMSE of all the bats



Bat algorithm utilizes a random path to produce new results from every chosen best solution in the local search, as follows:

$$X_{new} = X_{old} + \epsilon A^t \tag{6}$$

where $\epsilon \in [-1, 1]$ is a random number, and L^t represents the average loudness of all bat numbers at the current stage.

In terms of accuracy and performance, the Bat algorithm (BA) outperforms most other algorithms. The bat algorithm basically becomes the regular PSO if the frequency variations are replaced by a random parameter and $L_i = 1$ and $r_i = 1$ are set.

Table 4 Model-2: True and recovered model parameters of the composite interference gravity anomaly of a horizontal cylinder and a sphere model with corresponding RE and SD for each model parameter using the Bat algorithm

Model parameters	True value		Search range		Recovered value		RE (%)		SD		OF _{Obj}
	Horizontal cylinder model	Sphere model	Horizontal cylinder model	Sphere model	Horizontal cylinder model	Sphere model	Horizontal cylinder model	Sphere model	Horizontal cylinder model	Sphere model	
A (mGal.m ^{2q-μ})	50	250	10: 300	240	52	240	4	4	30.27	18.70	0.0002
z (m)	17	13	10: 20	12	16.20	12	4.70	7.69	3.31	1.87	
x_0 (m)	-50	50	-100: 100	50	-50	50	0	0	58.60	58.60	
q	1	1.5	0.5: 1.5	1.5	1	1.5	0	0	0.50	0.50	
$μ$	1	1	0: 1	1	1	1	0	0	0.70	0.70	

Forward modeling

Gravity anomaly at an observation point, x_j , along a profile (Fig. 1) is given by (Salem et al. 2004; Asfahani and Tlas 2008; Essa 2014):

$$g(x_j, x_0, z, \mu, q, A) = \frac{Az^\mu}{[(x_j - x_0)^2 + z^2]^q}, j = 1, 2, 3, \dots, n(7)$$

where x_j and x_0 represent the horizontal locations of the measured points and the origin of the buried source, z is the depth of the source, q is the shape factor (dimensionless), and A is the amplitude coefficient, whose dimension is determined by the shape factors (q and μ), yielding g in mGal units. The definitions of A , q , and μ for the above idealized bodies are shown in Table 1.

Materials and methods

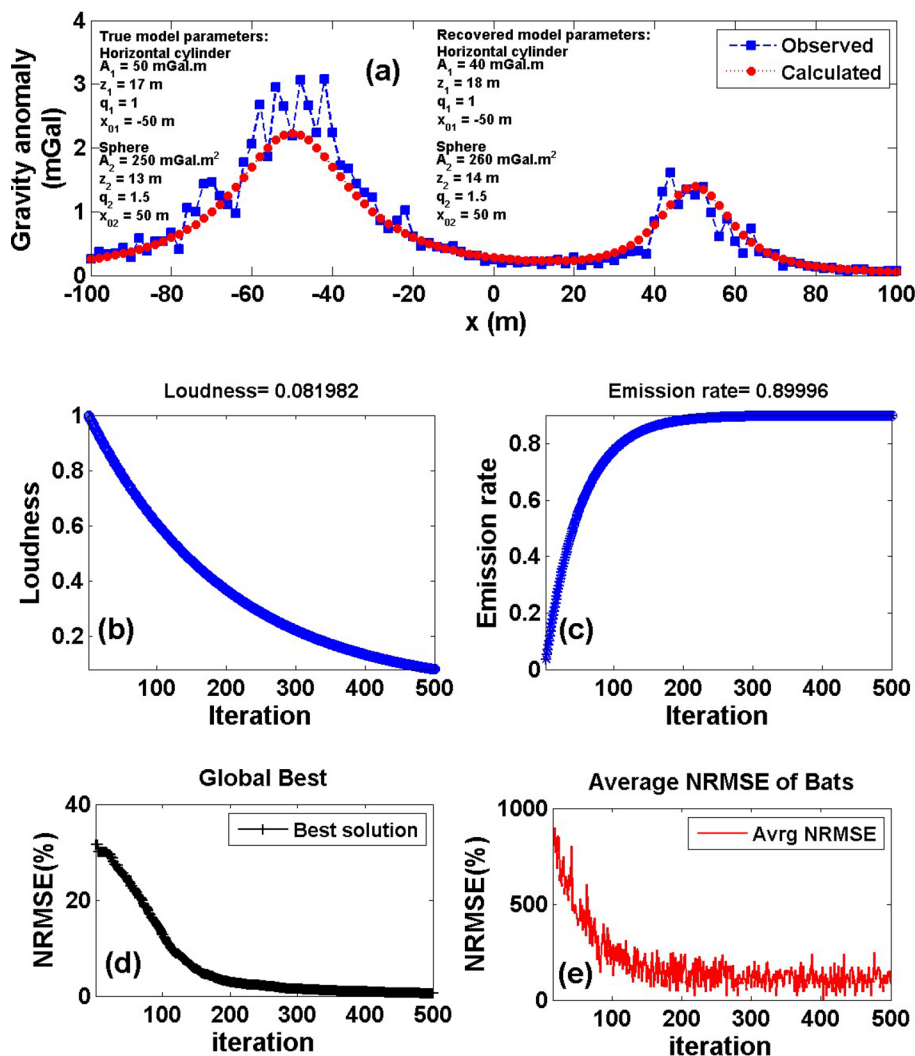
In gravity data interpretation, it is essential to obtain accurate results for the subsurface model parameters. Therefore, an inversion algorithm of large capacities is needed to accomplish accepted evaluations of subsurface model parameters such as depth, location, the shape of the buried body, etc. In various case studies, metaheuristic inversion methods have achieved promising results. Most metaheuristic inversion algorithms are quicker, easier, and more efficient than traditional inversion methods.

A new inversion Bat algorithm code was developed. The most significant parameters are depth, location, shape of the body, in addition to the amplitude coefficient (z , x_0 , q , A). Therefore, the proposed algorithm is searched to find an appropriate subsurface model that fits the actual data, i.e., assess the best-fit parameters. In general, each bat's location in search space represents a solution. Bats hover haphazardly in search space and implement a solution to each iteration. Each bat's position is determined using the optimum locations. The best location is the one that has the lowest misfit function value, and it is chosen as the best solution (X_{best}). The best solutions are then matched, and the best solution for every iteration is chosen. This process is repeated a pre-determined number of times. Finally, after the final iteration, the X_{best} is picked as the best solution. The Bat algorithm inversion code was first tested on various synthetic models in this research. After that, it was tested on real datasets.

The proposed algorithm that is utilized to invert the gravity data constitutes of the following procedures:

First step; The virtual bats' initial position X_i ($i = 1, 2, \dots, N$), frequencies Q_i , velocities V_i , loudness L_i , and the pulse rates r_i ; In the search space, each bat signifies a solution. X_i represents the variables of the characteristic source parameters [i.e., depth (z), origin (x_0), Amplitude coefficient

Fig. 7 Model-2: Noisy interference effect. **a** The noisy composite gravity anomaly generated by data set shown in Fig. 6a after adding 20% random Gaussian noise (True model parameters), as well as the calculated gravity response of them (Recovered model parameters) using the Bat algorithm technique, **b** loudness of the bats, **c** emission rat of the bats, **d** NRMSE of the global best solution (F_{Obj}) of the bats versus the iteration numbers, and **e** the average NRMSE of all the bats



(A), and shape factor (q) randomly selected from the search space, and V_i represents the velocity for each individual, virtual bat.

Second step; Finding the X_{best} .

The objective function (F_{Obj}) is defined as the normal root-mean-square (NRMSE) misfit error between the observed and calculated gravity data anomalies:

$$F_{Obj} = \frac{100}{\text{Max}(g_{obs}) - \text{Min}(g_{obs})} \sqrt{\frac{\sum_{j=1}^N [g_{obs} - g_{cal}]^2}{N}} \quad (8)$$

where, N is the total number of data points, g_{obs} is the observed gravity and g_{cal} is the calculated gravity. The g_{cal} is calculated by the forward modeling algorithm. Initially, Eq. 8 is applied to compute misfits, and then the bat with the minimum misfit is selected as the X_{best} .

Third step; While the program still doesn't reach the maximum number of iterations operate the following instructions:

Table 5 Model-2: True and recovered model parameters of the noisy composite interference gravity anomaly of a horizontal cylinder and a sphere model with corresponding RE and SD for each model parameters using the Bat algorithm

Model parameters	True value		Search range	Recovered value		RE (%)		SD		OF _{Obj}
	Horizontal cylinder model	Sphere model		Horizontal cylinder model	Sphere model	Horizontal cylinder model	Sphere model	Horizontal cylinder model	Sphere model	
A (mGal.m ^{2q-μ})	50	250	10: 300	40	260	20	4	30.27	47.60	0.0058
z (m)	17	13	10: 20	18	14	5.88	7.69	6.05	1.87	
x_0 (m)	-50	50	-100: 100	-50	50	0	0	58.60	58.60	
q	1	1.5	0.5: 1.5	1	1.5	0	0	0.50	0.50	
$μ$	1	1	0: 1	1	1	0	0	0.70	0.70	

- Adjust the frequency (Eq.1) and update the velocities and location/solutions to create a new solution (Eqs. 2 and 3).

- if $rand > r_i$

- choose a solution between the best solution.

- produce a local solution around the picked best solution (Eq.6), where $rand$ represents a random number with a uniform distribution.

- end if

- if $rand < L_i$ and $F_{Obj}(X_i) < F_{Obj}(X_{best})$

- admit the new solutions

- increase r_i and decrease L_i (Eqs. 4 and 5)

- end if

- Rank the bats and catch the current X_{best}

- end while

The Bat algorithm basic steps can be outlined in the pseudo-code illustrated in Fig. 2 and the flow chart shown in Fig. 3.

Results and discussion

Synthetic datasets

The introduced Bat algorithm was tested on two synthetic datasets to demonstrate its validity and accuracy in gravity data inversion. The synthetic responses are confined to the simple class of the geometrical shapes of vertical cylinder,

horizontal cylinder, and spheres. Then to prove the stability of the proposed Bat algorithm inversion approach, the inversions are performed on noisy data as well as interference effect model example.

Model 1

First, a noise-free simple synthetic example of a horizontal cylinder model has been inspected. The gravity effect of a horizontal cylinder model with input parameters: $A = 70$ mGal.m, $z = 15$ m, $x_0 = 0$ m and $q = 1$ is calculated using Eq. (7) with a 201-m long profile (Fig. 4a). Following the



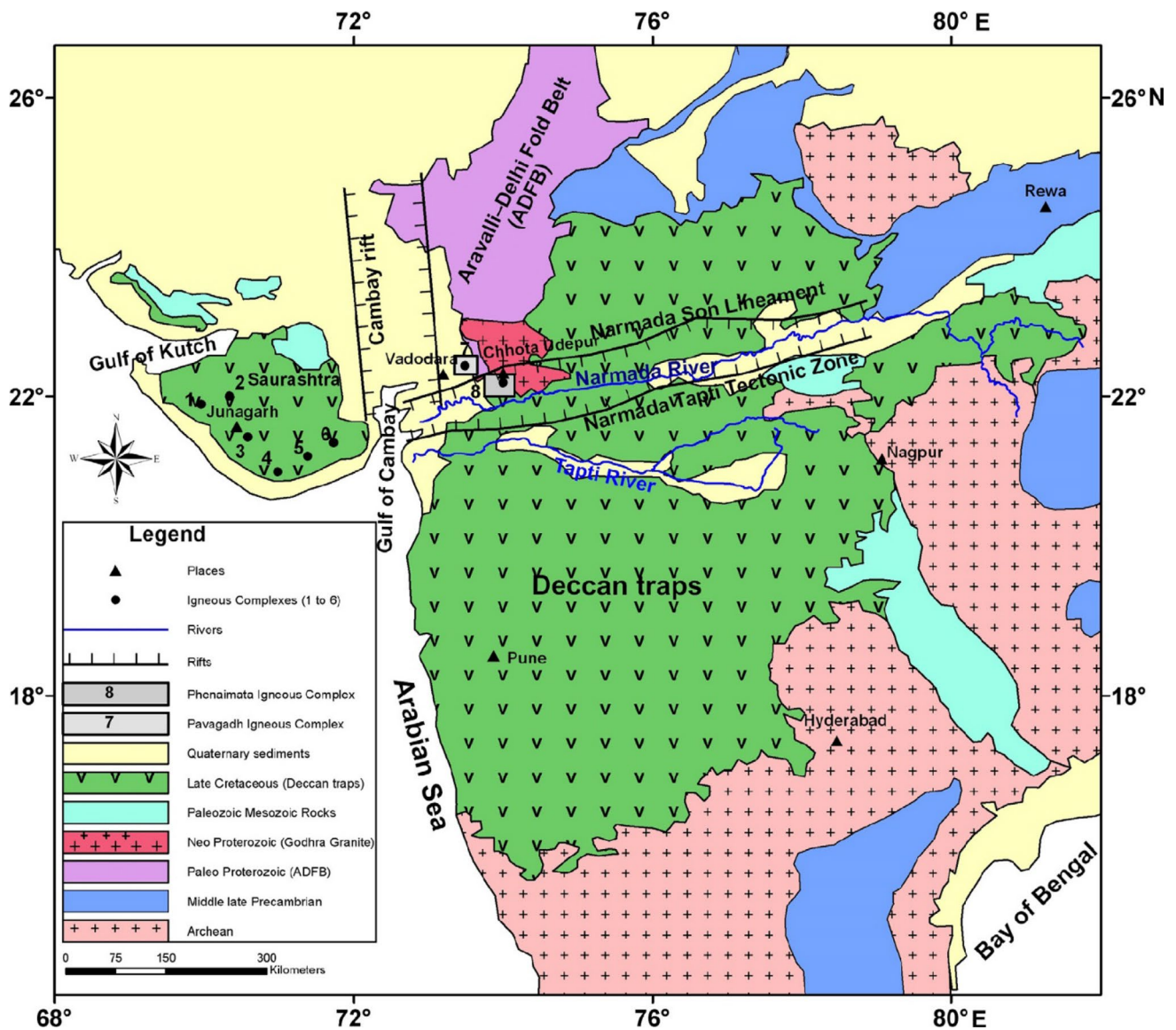


Fig. 8 Simplified geological and tectonic map of the Deccan traps (green) and adjacent area showing locations of some important igneous complexes in the NW and central India. Grey color rectangles

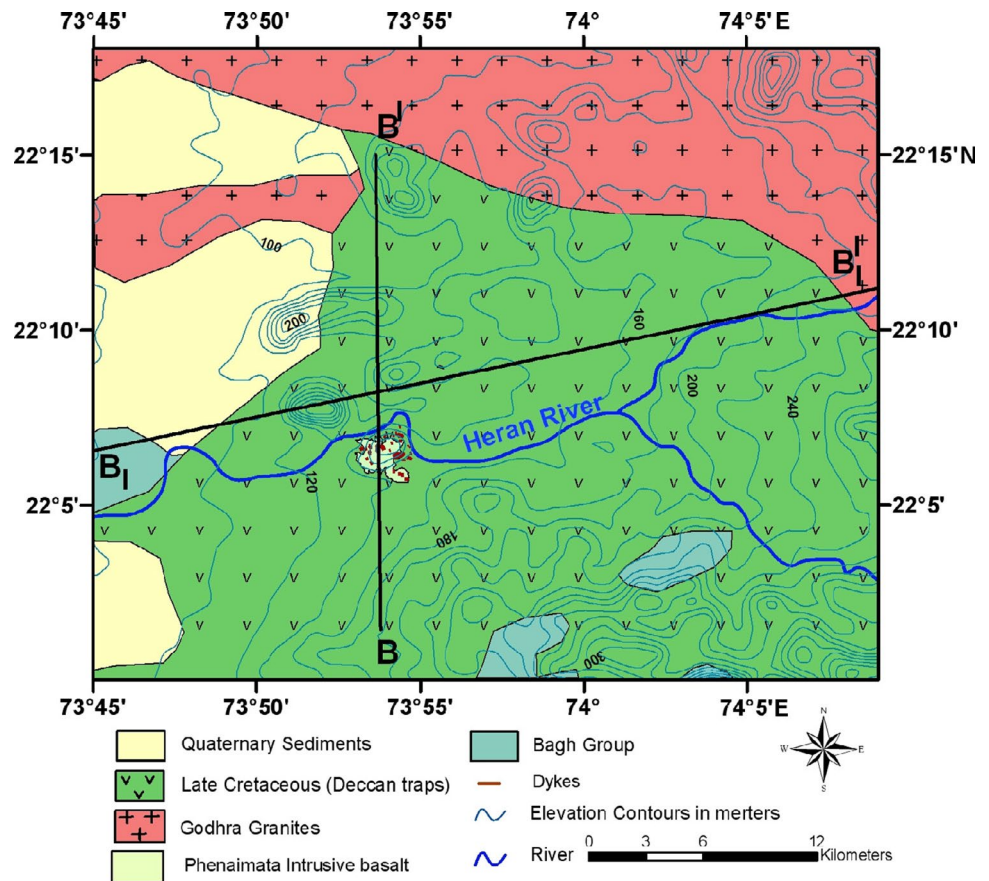
indicate the present study area covering Phenaimata igneous complex (after Krishnamurthy et al., 2000; Singh et al. 2014)

procedures of the Bat algorithm technique proposed in Sect. 2. Figure 4b shows the average loudness of all bat numbers obtained for several iterations. The number of iterations is determined based on reaching the minimum NRMSE and getting the best solution of the residual gravity anomaly (Fig. 4a). Figure 4c shows the emission rate of all bats obtained for every iteration process; the loudness of the bats decreases as they approach their prey; while the rate of pulse emission increases. Figure 4d shows the NRMSE of the global best solution (minimum objective function) vs.

the iteration numbers. The NRMSE reaches the minimum after the 500 iterations process for all bat numbers. Figure 4e shows the average NRMSE of all the bats obtained for every iteration process.

The global best solution of the gravity anomaly (i.e., model parameters) is obtained when the objective function (F_{Obj}) approaches the minimum of the NRMSE for the different iteration processes. Table 2 shows that the recovered model parameters of the proposed noise-free synthetic example are identical with the true-model parameters when

Fig. 9 Detailed geology and physiography of the area around Phenaimata igneous intrusive. BB' shows profile adopted for gravity interpretation using the Bat algorithm technique (after Hari et al. 2011; Singh et al. 2014)



the objective function (F_{Obj}) approaches the minimum. The result shows that the proposed Bat algorithm technique is stable and talented in recovering the true values of the model parameters of the buried model. Also, Table 2 illustrates the used search space for every model parameter, relative errors (RE), and the standard division (SD) of the given model. The search ranges are selected based on the aforementioned true-model parameters. Therefore, the search range should be approved to simulate more realistic examples where a priori information is absent.

A 20% random Gaussian noise has been added to the free-noise observed gravity anomaly (Fig. 5a) to test the proposed Bat algorithm stability. By applying the procedures of the Bat algorithm declared-above to the noisy data, the best results of the recovered model parameters will be corresponding to the minimum objective functions F_{Obj} (NRMSE). The loudness and emission rate of the bats are shown in Figs. 5b and c. Figures 5d and e depict the NRMSE of the global best solution (min objective function)

and the average NRMSE of all the bats. Table 3 shows that the recovered model parameters of the proposed noisy synthetic example (i.e., corresponding to min objective function F_{Obj}) are not significant influenced by the contaminated 20% random Gaussian noise, and recovered parameters are close to the true ones. As a result, it can be inferred that the BA technique suggested here is stable concerning for noise. The RE and SD of the recovered model parameters are illustrated in Table 3.

Model 2

The gravity data of an anomalous buried object can be impacted by an interfering effect (that is, the action of surrounding structures) in specific geologic contexts (Mehanee and Essa 2015). We computed the composite gravity response (using formula (7)) of two surrounding geologic objects, namely a horizontal cylinder model with true model values [$A_I = 50$ mGal.m, $z_I = 17$ m, $x_{0I} = -50$ m and $q_I = 1$]

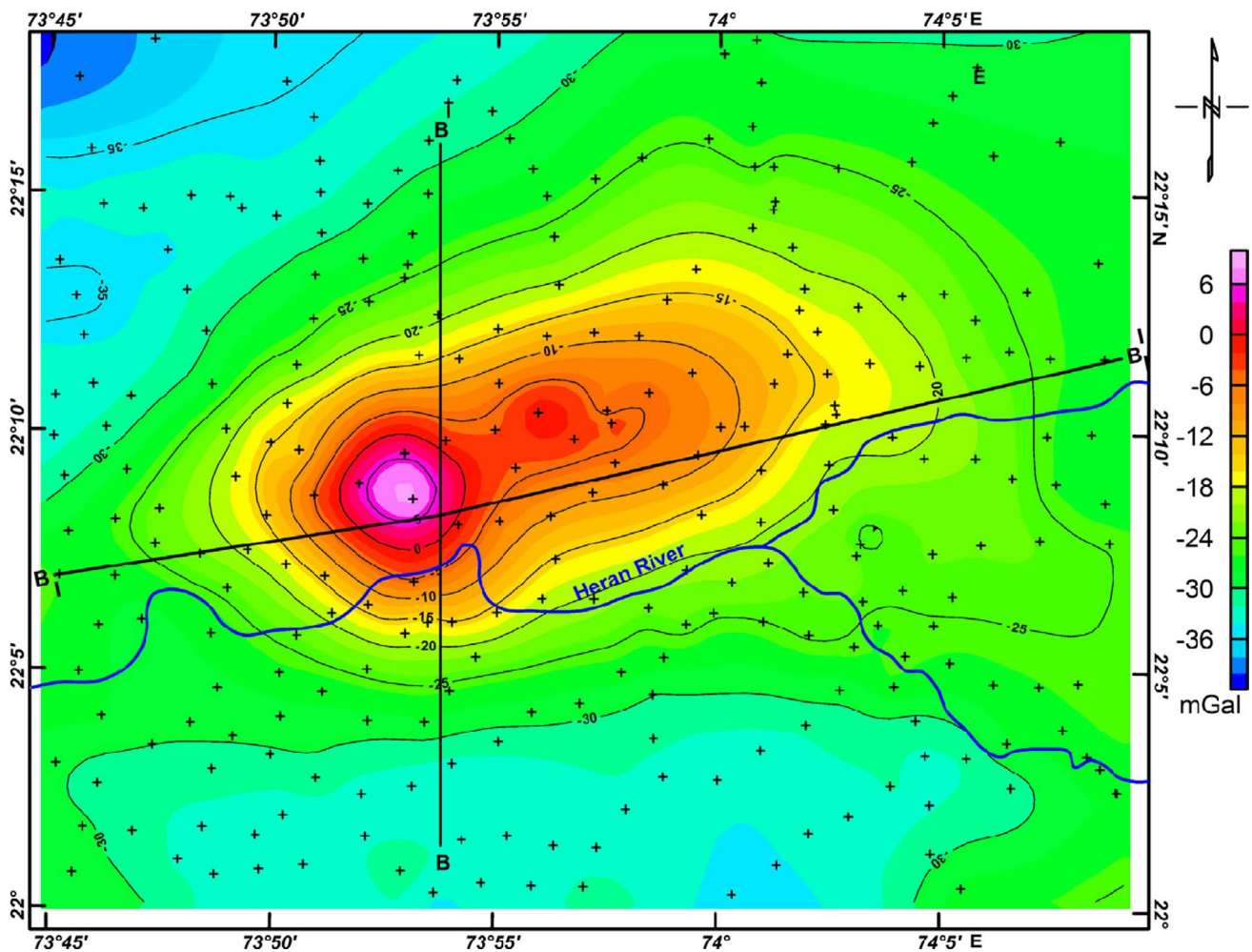
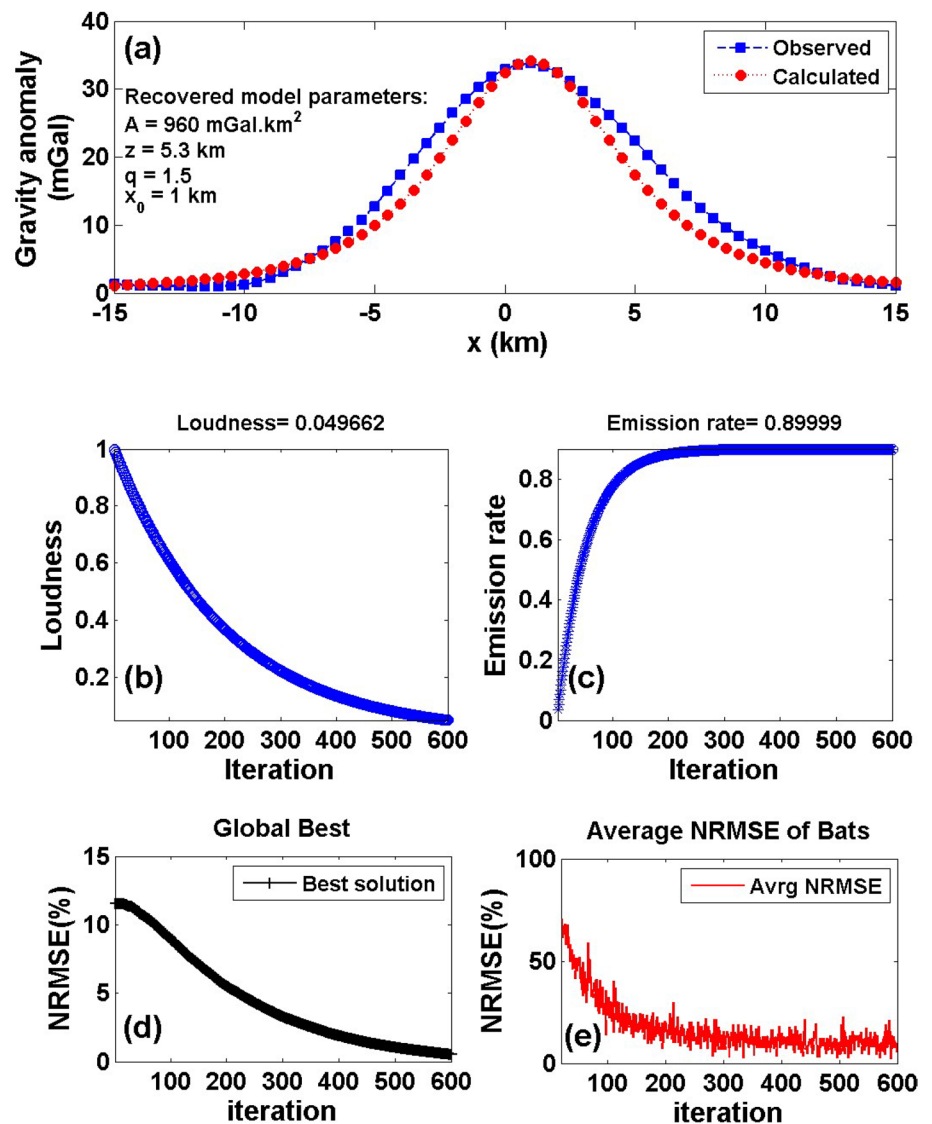


Fig. 10 Bouguer gravity anomaly map of Phenaimata igneous complex, Gujarat, India. + indicates gravity stations. BB' shows profile location adopted for gravity interpretation using the Bat algorithm technique (after Singh et al. 2014)

and a sphere model with true model values [$A_2 = 250$ mGal, m^2 , $z_2 = 17$ m, $x_{02} = 50$ m, and $q_2 = 1.5$], along a profile length of 201 m (Fig. 6a) to test this influence on the truthfulness of the characteristic parameters estimated from the Bat algorithm methodology presented here. Applying the procedures of the Bat algorithm technique described-above, the calculated gravity response of the two models is obtained in Fig. 6a. The obtained average loudness of the composite response is shown in Fig. 6b, while the emission rate of bat for the composite anomaly is shown in Fig. 6c. The NRMSE of the global best solution (min objective function, F_{Obj}) is given in Fig. 6d, and the average NRMSE of all the bats is shown in Fig. 6e. Figure 6 and Table 4 show that the Recovered model parameters of the two introduced models are identical to the true ones. This result supports that the Bat algorithm technique is stable in the cases of multi-structures relying on the extent of the neighboring effect.

To further investigate the procedure of BA on Multi-structure and surrounding effect, we contaminated the composite gravity response (Fig. 6a) with a noise level of 20% of random Gaussian noise (Fig. 7a). Figures 7b and c present the average loudness and emission rate of the bat to the overall composite gravity anomaly, respectively. Figures 7d and e show the NRMSE of the global best solution (min objective function, F_{Obj}), and the average NRMSE of all the bats, respectively. Figure 7a and Table 4 illustrate that the calculated composite anomaly and the recovered model parameters of the two introduced models even after being contaminated with noise. Also, they reveal that the recovered model parameters differ slightly from the true ones due to the effect of both the surrounded objects and noise. In general, the model parameters recovered using BA from the noisy interference sources for the first and second models are in good matching with the exact values (Table 5). These results support and confirm the Bat algorithm method find.

Fig. 11 The Phenaimata anomaly, Gujarat, India. **a** The observed gravity anomaly profile (blue squares), and the calculated best-fitting gravity response (red circles) using the Bat algorithm technique, **b** loudness of the bats, **c** emission rate of the bats, **d** NRMSE of the global best solution (F_{Obj}) of the bats versus the iteration numbers, and **e** the average NRMSE of all the bats



Based on the numerical models presented above, the method described here is stable and appropriate for field gravity data interpretation, as explained in the following section.

Table 6 The Phenaimata anomaly, Gujarat, India. Recovered model parameters with the corresponding minimum F_{Obj} and the SD for each parameter using the Bat algorithm

Model parameters	Search range	Recovered value	SD	OF_{Obj}
A (mGal.km ²)	800: 1100	960	87.03	0.0002
z (km)	3: 7	5.3	1.58	
x_0 (km)	- 15: 15	1	8.87	
q	0.5: 1.5	1.5	0.50	
μ	0: 1	1	0.71	

Field datasets

Two field cases for geothermal investigation and volcanic activity study are analyzed to examine the applicability of the established methodology.

The Phenaimata gravity anomaly, Gujarat, India

The Phenaimata igneous complex lies northern the Narmada River and is part of the Narmada-Tapti tectonic zone (NTTZ) (Fig. 8). The Narmada rift appears to regulate the positioning of this plug-like entity. This intrusive is located 23 km southwest of Chhota Udaipur, on the left bank of the Heran River (Fig. 9). It's also a bimodal igneous complex, with plutonic and volcanic rock types representing tholeiitic and alkaline magmatism. Basalt, layered gabbro, diorite, nepheline-syenite, lamprophyres, and granophyres make up the Phenaimata plug, which is a differentiated igneous complex



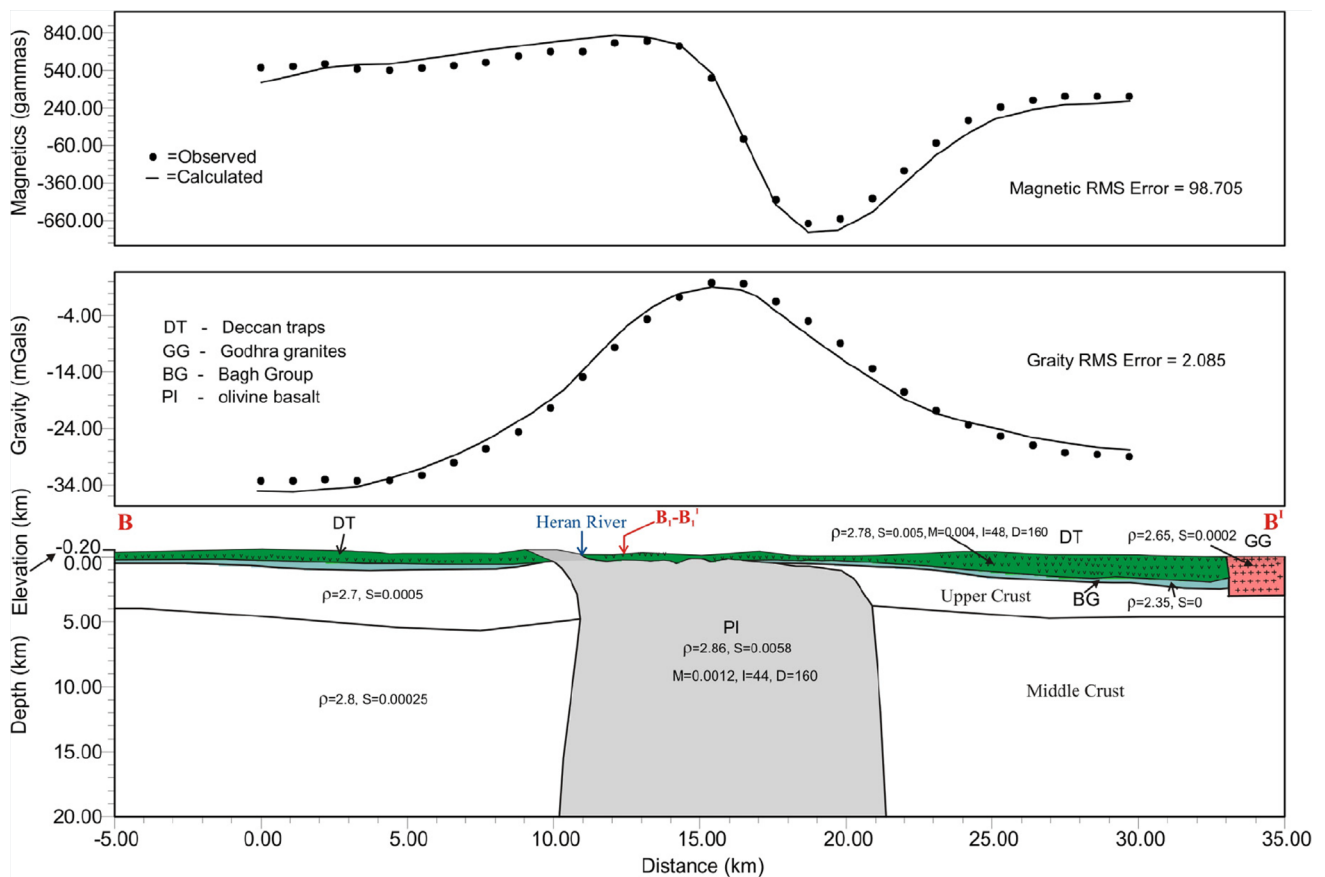


Fig. 12 Results of 2.5 D joint modeling of Gravity–Magnetic anomalies along N-S profile BB' over the Phenaimata intrusive complex Bougeur gravity map. Where ρ is density, S is susceptibility and M is magnetization are given in CGS units (after Singh et al. 2014)

(Sukeshwala and Sethna 1969; Hari et al. 2011 and 2014). The Phenaimata complex is made up of two-thirds basalts and one-third alkaline plutonic series. The Phenaimata igneous complex produced orthopyroxene gabbro, according to Hari et al. (2011). According to the petrological modeling, the origin of gabbroic rocks was caused by magma accumulation in the crust, contemporaneous assimilation, and fractional crystallization. Also, reverse magnetization has been found in olivine gabbro and syenite rocks and implying emplacement toward the end of the major Deccan volcanism period in the Phenaimata igneous complex (Basu et al. 1993; Poornachandra Rao et al. 2004).

The Bouguer gravity anomaly map in the Phenaimata igneous exposure displays an elliptical-shaped anomaly closure to the North of the complex, with the principal axis of the anomalies aligned roughly in the ENE–WSW direction, which aligns with the Narmada-Tapti tectonic zone's orientation (Fig. 10). A north–south BB' 30 km long profile was

taken perpendicular to the closure anomaly of the Bouguer gravity map using a 0.5 km sample interval. The BB' residual gravity anomaly profile (Fig. 11a) was obtained after separating the regional anomaly from the BB' Bouguer gravity anomaly profile using a suitable separation technique.

The Bat algorithm methodology was applied to the residual gravity anomaly using the probable search range of the characteristic parameters (Table 6). Figures 11b and c illustrate the average bat loudness and emission rate for the residual gravity profile, respectively. Figures 11d and e illustrate the NRMSE of the global best solution ($\min F_{Obj}$) and the average NRMSE of all bats, respectively. The best optimum model parameters correspond to the $\min F_{Obj}$. The minimum F_{Obj} is 0.0002 mGal, and the best model parameters are [$A = 960$ mGal.km, $z = 5.3$ km, $x_0 = 1$ km, $q = 1.5$, and $\mu = 1$], which recommend that the intrusive body of the Phenaimata igneous complex anomaly is approximated by sphere like model (Table 6).



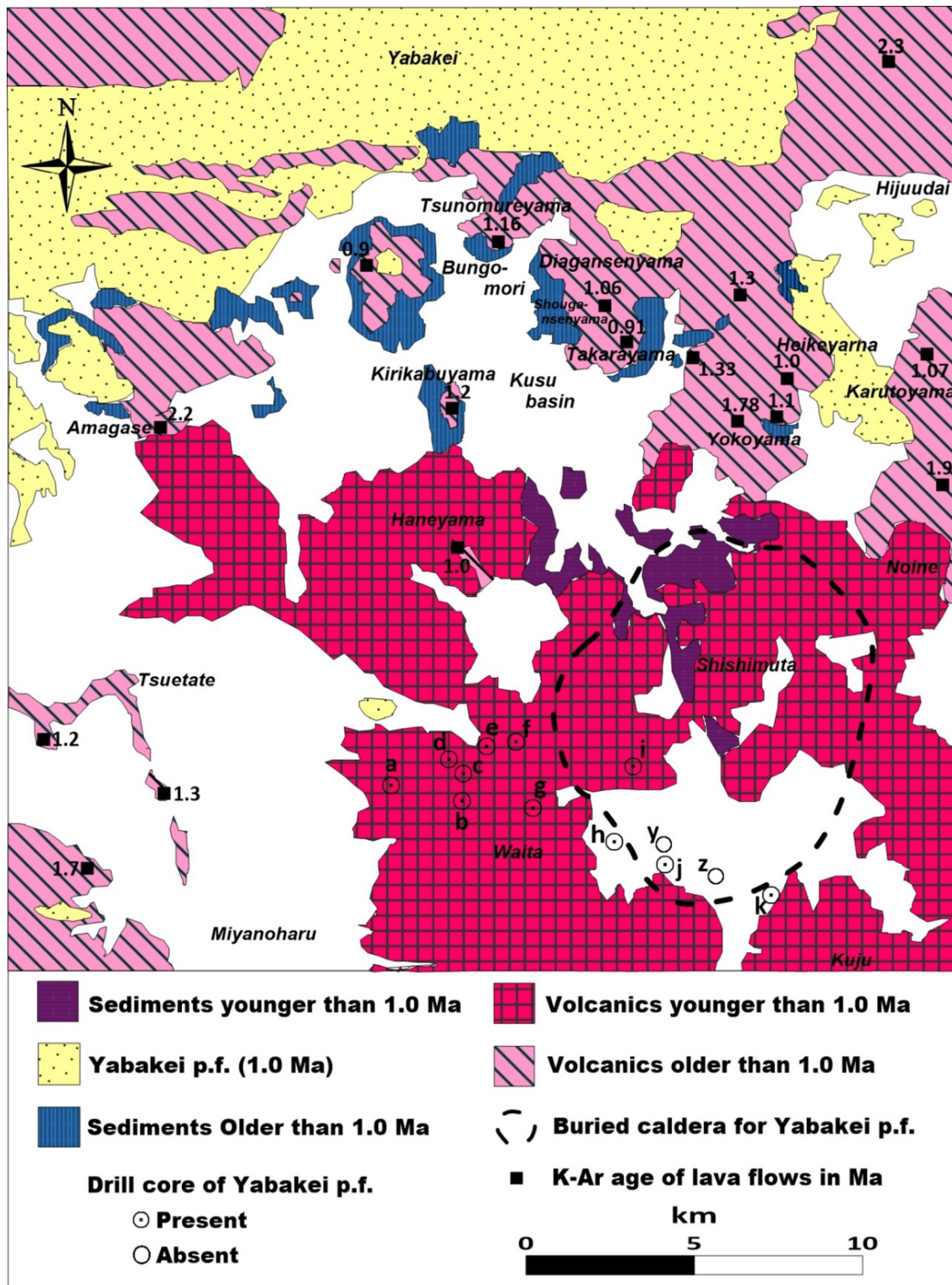


Fig. 13 Geologic map of the Kusu basin and Shishimuta area of the Hoho volcanic zone, Kyushu, Japan (modified after Kamata 1989b). Dotted circles represent the locations of drill holes and opened circles refer to the location of 3000- m deep drill holes with spot coring



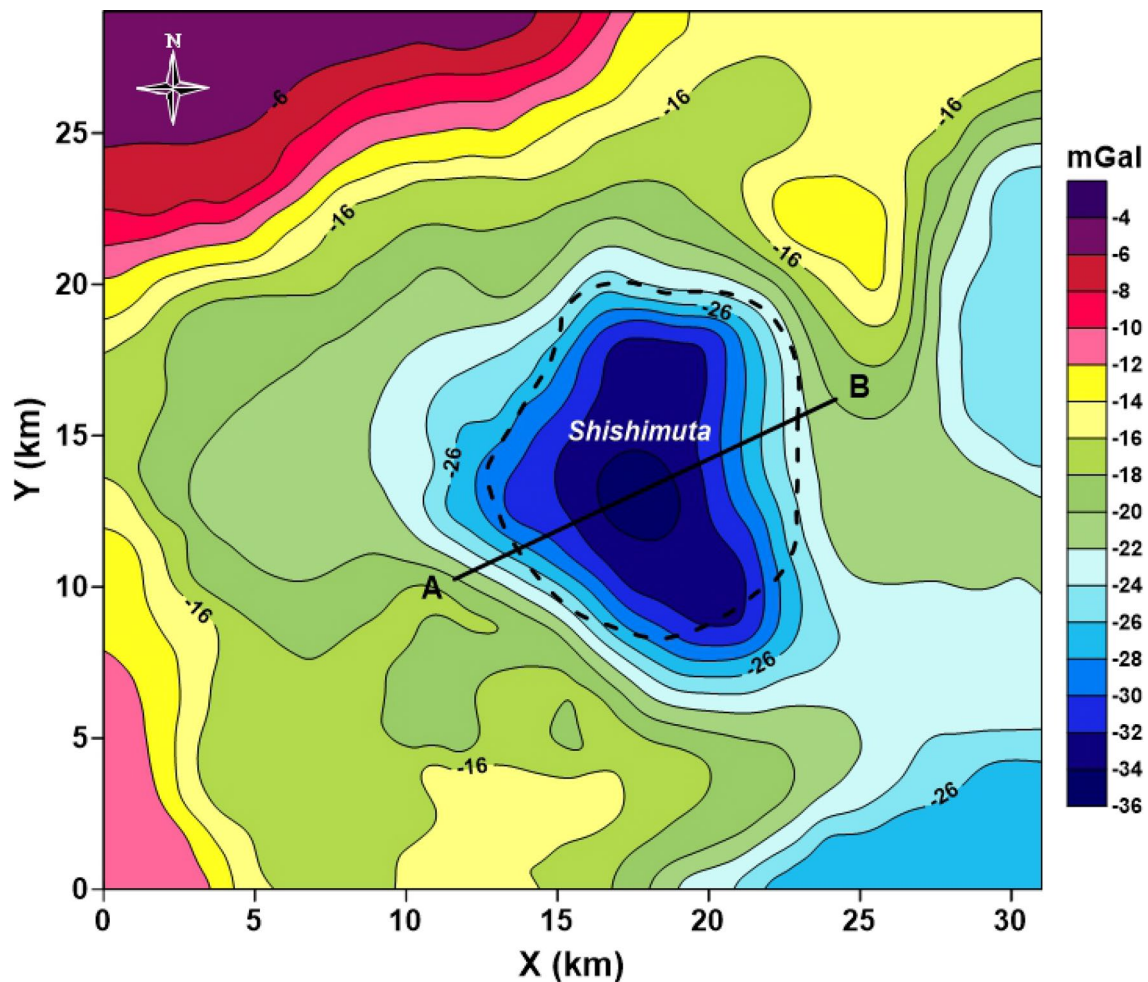


Fig. 14 Bouguer gravity map of the central part of Hoho volcanic zone, Kyushu, Japan. Contour interval is 2 mGals. Assumed density is 2.3 g/cm^3 . The dotted line refers to the location of the Shishimuta

caldera (modified after Kornazawa and Kamata 1985). The gravity anomaly profile (Fig. 15a) subjected to interpretation using the Bat algorithm is denoted by AB

The measured and computed gravity anomalies of the Phenaimata igneous complex anomaly are in good agreement, as shown in Fig. 11a. Using a density of the volcanic intrusive rock (Gabbro) of 2.86 g/cm^3 and average density of the surrounding rocks of 2.65 g/cm^3 , then the density contrast ($\Delta\rho$) is 0.21 g/cm^3 according to Singh et al. (2014), the depth to the top will be 2.76 km, which is in good agreement with the results obtained by joint modeling of Singh et al. (2014) (Fig. 12).

The Hoho volcanic gravity anomaly, Kyushu, Japan

The Hoho volcanic zone in central Kyushu, southwest Japan, is a 70 km long, 45 km wide volcano-tectonic depression with Plio-Pleistocene volcanic materials widely dispersed in an E-W orientation. With a limited amount of volcanic-clastic material, these volcanic rocks are mostly made up of andesitic lava flows and dacitic pyroclastic-flow deposits.

From around 5 Ma to the present, the Hoho volcanic zone provides a strong indication that volcanic activity and subsidence alternated under a regional extensional stress field, with the depression mainly remunerated by filling of an equal amount of volcanic material (Kamata 1989a, b).

Based on drill-hole, geochronologic, and gravity data, the buried Shishimuta caldera was identified beneath post-caldera lava domes and lacustrine deposits in the center of the Hoho volcanic zone. The Yabakei pyroclastic flow, which erupted 1.0 Ma ago with a bulk volume of 110 km^3 , is the source of the Shishimuta caldera in the center of the Hoho volcanic zone (Fig. 13). The Shishimuta caldera is an 8-km wide, 3-km deep breccia-filled funnel depression with a V-shaped negative Bouguer gravity anomaly of up to 36 mGal (Fig. 14). The andesitic breccia fills the caldera and has a relatively low density; it was likely produced by fragmentation of disturbed ceiling rock during the intense Yabakei eruption and subsequent collapse (Aramaki 1984).



Fig. 15 The Hoho volcanic anomaly, Kyushu, Japan. **a** The observed gravity anomaly profile (blue squares), and the calculated best-fitting gravity response (red circles) using the Bat algorithm technique, **b** loudness of the bats, **c** emission rate of the bats, **d** NRMSE of the global best solution (F_{Obj}) of the bats versus the iteration numbers, and **e** the average NRMSE of all the bats

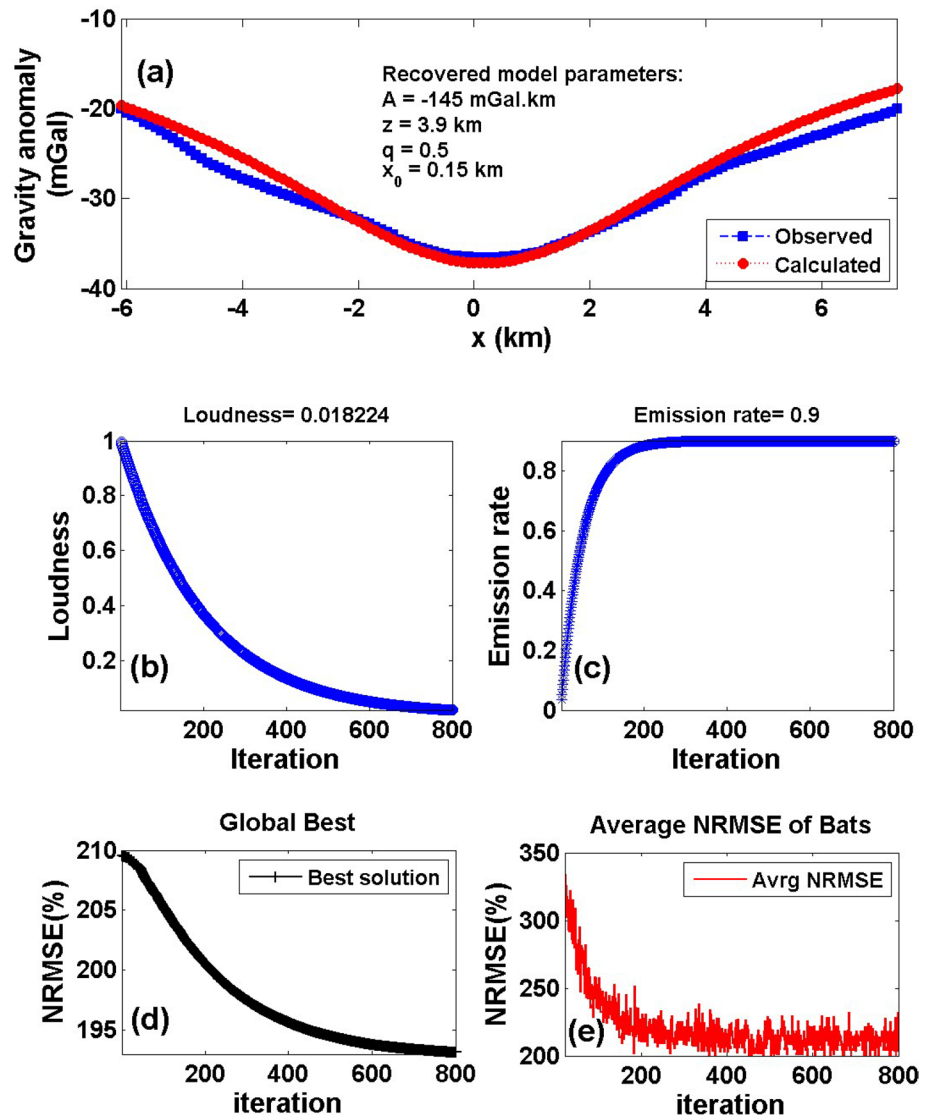


Table 7 The Hoho volcanic anomaly, Kyushu, Japan. Recovered model parameters with the corresponding minimum F_{Obj} and the SD for each parameter using the Bat algorithm

Model parameters	Search range	Recovered value	SD	OF_{Obj}
A (mGal.km)	-105: -205	-145	29.58	0.0043
z (km)	1.5: 10.5	3.9	2.64	
x_0 (km)	-6.1: 7.3	0.15	3.91	
q	0.5: 1.5	0.5	0.50	
μ	0: 1	0	0.71	

Komazawa and Kamata (1985) and Kamata (1989a, b) introduced a gravity model that defined the V-shaped depression with depth to the Pre-Tertiary basement up to 3.8 km below sea level.

A NE-SW AB profile was taken normal to the trend of the Shishimuta caldera anomaly of the previous Bouguer

gravity map to be subjected to the BA interpretation procedures (Fig. 15). The AB Bouguer gravity anomaly profile with a length of 13.5 km was digitized at 0.1 km sampling intervals (Fig. 15a).

The Bat algorithm interpretation procedures have been applied to the AB anomaly profile of the Shishimuta caldera of the Hoho volcanic zone using the suitable search range of the characteristic parameters. Figures 15b and c demonstrate the average bat loudness and emission rate for the Bouguer gravity profile, respectively. Figures 15d and e demonstrate the NRMSE of the global best solution (min F_{Obj}) and the average NRMSE of all bats, respectively. Note, the increase in the NRMSE of the objective function (F_{Obj}) is due to work directly on the Bouguer gravity anomaly profile instead of the residual gravity anomaly profile in the other field example mentioned-above. The best interpretive model parameters correspond to the min F_{Obj} . The minimum F_{Obj} is 0.0043 mGal, and the best-recovered model parameters are

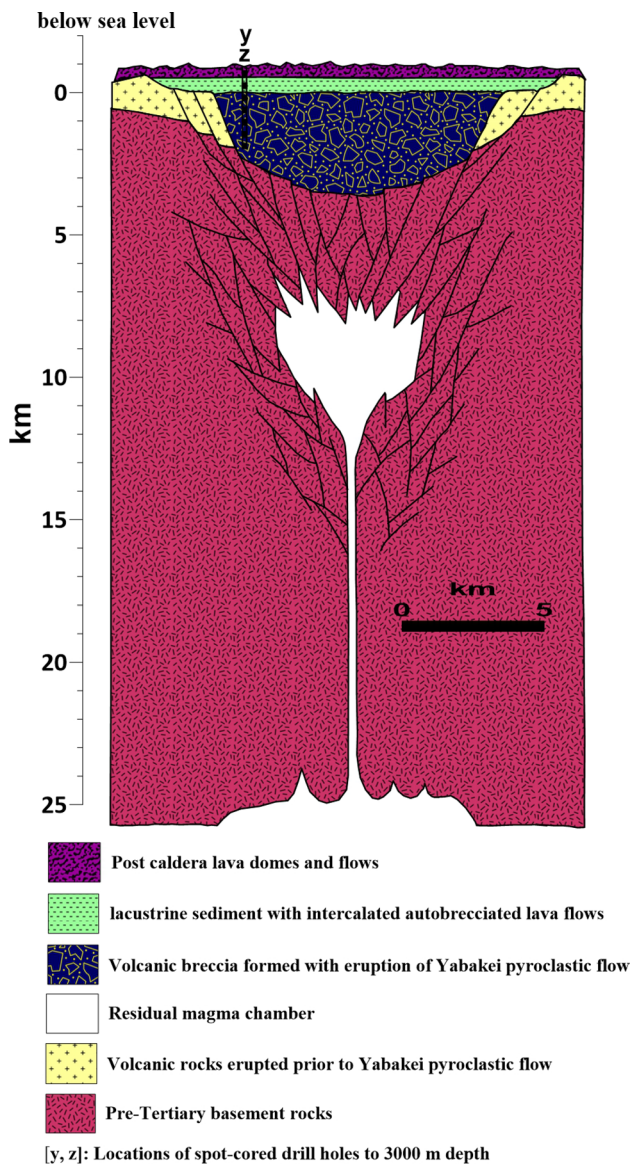


Fig. 16 Interpretive N-S profile of the Shishimuta caldera (modified after Kamata 1989b)

[$A = -145$ mGal.km, $z = 3.9$ km, $x_0 = 0.15$ km, $q = 0.5$, and $\mu = 0$], which recommend that the source of the Shishimuta caldera anomaly is approximated by vertical cylinder-like model (Table 7). Figure 15a shows great matching between the observed and calculated anomaly.

Drill holes outside Shishimuta caldera (boreholes with dotted circles; a – k in Fig. 13) encounter Pre-Tertiary rocks at depths of 2.0–2.5 km (Sasada 1984; Tamanyu 1985).

While drill holes up to 3 km deep within the caldera (boreholes with opened circles; y and z in Fig. 13), on the other hand, penetrate Plio-Pleistocene volcanic rocks instead of Pre-Tertiary materials (MITI 1986). According to depth modeling to gravity basement of the caldera, Komazawa and Kamata (1985) and Kamata (1989a, b) suggest the Pre-Tertiary rocks lie about 3.8 km underneath the surface (Fig. 16). The proposed technique of BA interpreted the depth to Pre-Tertiary basement rocks of the caldera about 3.9 km, which agree very well with the drilling and modeling information of Kamata (1989a, b) and Komazawa and Kamata (1985).

Conclusion

Estimation of an appropriate and precise model for representing the subsurface structures is critical in gravity data interpretation. The inversion process, which involved model parameter estimation, represents the main stage in the geophysical data analysis and interpretation and produces an appropriate model relying on the physical characteristic of the deliberated environment. A new metaheuristic algorithm called the Bat algorithm, based on the echolocation behavior of bats, was applied to gravity data to obtain the best convenient characteristic parameters and discover a satisfactory model. The best-interpreted model parameters (depth, origin location, amplitude coefficient, and geometric shape factor) are obtained corresponding to the minimum objective function after reaching the global best solution. The BA technique does not require a priori information; The developed inversion technique of the BA is simple, fast, accurate, and easy to be applied to gravity datasets. Furthermore, the appropriate efficiency and accuracy of the proposed BA technique have been confirmed on synthetic datasets with noise-free & noisy examples, as well as on multiple structures to test the interference effect. Finally, the BA technique is successfully applied to two field data examples from India and Japan for geothermal exploration and volcanic activity study. The inverted outcomes of the BA technique are found in good agreement with the available drilling & geological information and the published literatures. We concluded that the proposed technique is helpful in geothermal investigations and the study of volcanic activity and we recommend that the proposed technique of BA can extend to mineral & ore exploration in future studies.

Acknowledgements The authors wish to thank the editor-in-chief prof. Madjid Abbaspour to submit the manuscript to be published in International Journal of Environmental Science and Technology and the anonymous reviewers on their careful comments.

Author contributions Essa K.S. contributed in writing the original manuscript draft, conceptualization, methodology, figures and tables preparations. Diab Z.E. contributed in writing the original manuscript draft, conceptualization, methodology, code validation, figures and tables preparations.

Declarations

Conflict of interests The authors declare that they have no known competing interests. There are no financial or non-financial interests that are directly or indirectly related to the work submitted for publication.

Data availability The authors declare that the data is available upon request.

References

- Abdelrahman EM, Essa KS (2015) Three least-squares minimization approaches to interpret gravity data due to dipping faults. *Pure Appl Geophys* 172:427–438
- Abdelrahman EM, El-Araby TM, Essa KS (2003) Shape and depth solutions from third moving average residual gravity anomalies using the window curves method. *Kuwait J Sci Eng* 30:95–108
- Al-Garni MA (2008) Walsh transforms for depth determination of a finite vertical cylinder from its residual gravity anomaly. *SAGEEP* 6–10:689–702
- Aramaki S (1984) Formation of the Aira caldera, southern Kyushu, 22000 years ago. *J Geophys Res* 89:8485–8501
- Asfahani J, Tlas M (2008) An automatic method of direct interpretation of residual gravity anomaly profiles due to spheres and cylinders. *Pure Appl Geophys* 165:981–994
- Asfahani J, Tlas M (2012) Fair function minimization for direct interpretation of residual gravity anomaly profiles due to spheres and cylinders. *Pure Appl Geophys* 169:157–165
- Asfahani J, Tlas M (2015) Estimation of gravity parameters related to simple geometrical structures by developing an approach based on deconvolution and linear optimization techniques. *Pure Appl Geophys* 172:2891–2899
- Athens N, Caers JK (2021) Gravity inversion for geothermal exploration with uncertainty quantification. *Geothermics* 97:102230
- Basu AR, Renne PR, Dasgupta DK, Teichmann F, Poreda RJ (1993) Early & late alkali igneous pulses and a high-3He plume origin for the Deccan flood basalts. *Science* 261:902–906
- Biswas A (2015) Interpretation of residual gravity anomaly caused by simple shaped bodies using very fast simulated annealing global optimization. *Geosci Front* 6:875–893
- Biswas A (2016) Interpretation of gravity and magnetic anomaly over thin sheet-type structure using very fast simulated annealing global optimization technique. *Model Earth Syst Environ* 2:30
- Casallas-Moreno KL, González-Escobar M, Gómez-Arias E, Mastache-Román EA, Gallegos-Castillo CA, González-Fernández A (2021) Analysis of subsurface structures based on seismic and gravimetric exploration methods in the Las Tres Vírgenes volcanic complex and geothermal field, Baja California Sur. *Mexico Geothermics* 92:102026
- Cooper G (2021) Iterative Euler. *Deconvolution Explor Geophys* 52:468–474
- Dorigo M, Maniezzo V, Colomi A (1996) The ant system: optimization by a colony of cooperating agents. *IEEE Trans Syst Man Cybern Part B* 26:29–41
- Dorigo M, Stützle T (2003) The Ant Colony Optimization Metaheuristic: Algorithms, Applications, and Advances. In: Glover F, Kochenberger GA, (eds) *Handbook of Metaheuristics*. International Series in Operations Research & Management Science, vol 57. Springer, Boston, MA. https://doi.org/10.1007/0-306-48056-5_9
- Ekinci YL, Yiğitbaş E (2015) Interpretation of gravity anomalies to delineate some structural features of biga and gelibolu peninsulas, and their surroundings (north-west Turkey). *Geodin Acta* 27:300–319
- Ekinci YL, Balakaya C, Gokturkler G, Turan S (2016) Model parameter estimations from residual gravity anomalies due to simple-shaped sources using Differential Evolution Algorithm. *J Appl Geophys* 129:133–147
- Eshabli AS, Osagie AU, Ismail NA, Ghanush HB (2021) Analysis of gravity and aeromagnetic data to determine structural trend and basement depth beneath the Ajdabiya Trough in northeastern Libya. *SN Appl Sci* 3:228
- Essa KS (2013) Gravity interpretation of dipping faults using the variance analysis method. *J Geophys Eng* 10:015003
- Essa KS (2014) New fast least-squares algorithm for estimating the best-fitting parameters of some geometric-structures to measured gravity anomalies. *J Adv Res* 5:57–65
- Essa KS (2021) Evaluation of the parameters of fault-like geologic structure from the gravity anomalies applying the particle swarm. *Environ Earth Sci* 80:489
- Essa KS, Géraud Y (2020) Parameters estimation from the gravity anomaly caused by the two-dimensional horizontal thin sheet applying the global particle swarm algorithm. *J Pet Sci Eng* 193:107421
- Essa KS, Munsch M (2019) Gravity data interpretation using the particle swarm optimization method with application to mineral exploration. *J Earth Syst Sci* 128:123
- Essa KS, Mehane SA, Soliman KS, Diab ZE (2020) Gravity profile interpretation using the R-parameter imaging technique with application to ore exploration. *Ore Geol Rev* 126:103695
- Essa KS, Abo-Ezz ER, Géraud Y (2021a) Utilizing the analytical signal method in prospecting gravity anomaly profiles. *Environ Earth Sci* 80:591
- Essa KS, Géraud Y, Diraison M (2021b) Fault parameters assessment from the gravity data profiles using the global particle swarm optimization. *J Pet Sci Eng* 207:109129
- Fister IJ (2013) A comprehensive review of bat algorithms and their hybridization. M.Sc. thesis: University of Maribor, Slovenia.
- Florio G (2020) The Estimation of Depth to Basement Under Sedimentary Basins from Gravity Data: Review of Approaches and the ITRESC Method, with an Application to the Yucca Flat Basin (Nevada). *Surv Geophys* 41:935–961
- Hari KR, Chalapathi Rao NV, Swarnkar V (2011) Petrogenesis of gabbro and orthopyroxene gabbro from the Phenai mata igneous complex, Deccan volcanic province: products of concurrent assimilation and fractional crystallization. *J Geol Soc India* 78:501–509
- Hari KR, Chalapathi Rao NV, Swarnkar V, Hou G (2014) Alkali feldspar syenites with shoshonitic affinities from Chhotadepur area: implication for mantle metasomatism in the Deccan large igneous province. *Geosci Front* 5:261–276
- Hinze WJ, von Frese RRB, Saad AH (2013) Gravity and magnetic exploration: principles, practices and applications. Cambridge University Press, Cambridge
- Hiramatsu Y, Sawada A, Kobayashi W, Ishida S, Hamada M (2019) Gravity gradient tensor analysis to an active fault: a case study at the Togi-gawa Nangan fault, Noto Peninsula, central Japan. *Earth Planets Space* 71:107



- Holland JH (1984) Genetic Algorithms and Adaptation. In: Selfridge OG, Rissland EL, Arbib MA (eds) Adaptive Control of III-Defined Systems. NATO Conference Series (II Systems Science), vol 16. Springer, Boston, MA. https://doi.org/10.1007/978-1-4684-8941-5_21
- Kaftan İ (2017) Interpretation of magnetic anomalies using a genetic algorithm. *Acta Geophys* 65:627–634
- Kamata H (1989a) Volcanic and structural history of the Hoho volcanic zone, central Kyushu, Japan. *Bull Volcanol* 51:315–332
- Kamata H (1989b) Shishimuta caldera, the buried source of the Yabakei pyroclastic flow in the Hoho volcanic zone, Japan. *Bull Volcanol* 51:41–50
- Karaboga D, Basturk B (2008) On the performance of artificial bee colony (ABC) algorithm. *Appl Soft Comput* 8:687–697
- Kaveh A, Farhoudi N (2013) A new optimization method: dolphin echolocation. *Adv Eng Software* 59:53–70
- Kennedy J, Eberhart R (1995) Particle swarm optimization. In: Proceedings of IEEE international conference on neural networks, pp. 1942–1948
- Kirkpatrick S, Gelati CD, Vecchi MP (1983) Optimization by simulated annealing. *Science* 220:671–680
- Komazawa M, Kamata H (1985) The basement structure of the Hoho Geothermal Area obtained by gravimetric analysis in central-north Kyushu, Japan. *Reports, Geol Surv Japan* 264:305–333 ((in Japanese))
- Li Y, Oldenburg D (1998) 3-D inversion of gravity data. *Geophysics* 63:109–119
- Lichoro CM, Arnason K, Cumming W (2019) Joint interpretation of gravity and resistivity data from the Northern Kenya volcanic rift zone: Structural and geothermal significance. *Geothermics* 77:139–150
- Mehanee S, Essa KS (2015) 2.5-D regularized inversion for the interpretation of residual gravity data by a dipping thin sheet: numerical examples and case studies with an insight on sensitivity and non-uniqueness. *Earth Planets Space* 67:130
- Mirjalili S, Mirjalili SM, Yang X-S (2014) Binary Bat Algorithm. *Neural Comput Appl* 25:663–681
- MITI (Ministry of International Trade and Industry) (1986) Report on the confirmation study of the effectiveness of prospecting for deep geothermal resources integrated analyses (3rd ver). Ministry International Trade Industry p:1–151 (in Japanese)
- Montesinos FG, Arnoso J, Vieira R (2005) Using a genetic algorithm for 3-D inversion of gravity data in Fuerteventura (Canary Islands). *Int J Earth Sci* 94:301–316
- Pace F, Santilano A, Godio A (2021) A review of geophysical modeling based on particle swarm optimization. *Surv Geophys* 42:505–549
- Pallero JLG, Fernández-Martínez JL, Bonvalot S, Fudym O (2017) 3D gravity inversion and uncertainty assessment of basement relief via Particle Swarm Optimization. *J Appl Geophys* 139:338–350
- Poornirzaee R, Sarmady S, Sharghi Y (2019) A new inversion method using a modified bat algorithm for analysis of seismic refraction data in dam site investigation. *J Environ Eng Geophys* 24:201–214
- Poornirzaee R (2017) Applying bat metaheuristic algorithm for building shear wave velocity models from surface wave dispersion curves: in 23rd European Meeting of Environmental and Engineering Geophysics, Sweden, 1–5
- Poornachandra Rao GVS, Mallikharjun Rao J, Jaya Prasanna Lakshmi K (2004) Palaeomagnetic study of the alkaline rocks associated with the Deccan traps of north western India. *Indian J Geochem* 19:19–32
- Rashedi E, Nezamabadi S, Saryazdi S (2009) GSA: a gravitational search algorithm. *Inf Sci* 179:2232–2248
- Rathee N, Chhillar RS (2020) Gravitational search algorithm: a novel approach for structural test path optimization. *J Interdiscip Math* 23:471–480
- Roshan R, Singh UK (2017) Inversion of residual gravity anomalies using tuned PSO. *Geosci Instrum Methods Data Syst* 6:71–79
- Salem A, Ravat D, Mushuyandebvu MF, Ushijima K (2004) Linearized least-squares method for interpretation of potential field data from sources of simple geometry. *Geophysics* 69:783–788
- Sarsar Naouali B, Guellala R, Bey S, Inoubli MH (2017) Gravity data contribution for petroleum exploration domain: mateur case study (Saliferous Province, Northern Tunisia). *Arab J Sci Eng* 42:339–352
- Sasada M (1984) Basement structure of the Hoho geothermal area, central Kyushu, Japan. *J Japan Geotherm Energy Assoc* 21:1–11 ((in Japanese))
- Singh B, Prabhakara Rao MRK, Prajapati SK, Swarnapriya Ch (2014) Combined gravity and magnetic modeling over Pavagadh and Phenaimata igneous complexes, Gujarat, India: Inference on emplacement history of Deccan volcanism. *J Asian Earth Sci* 80:119–133
- Snowden DV, Glacken I, Noppe MA (2002) Dealing with demands of technical variability and uncertainty along the mine value chain. In Proceedings, Value Tracking Symposium. Australas Inst Min Metall 2002:93–100
- Storn R, Price K (1997) Differential evolution—a simple and efficient heuristic for global optimization over continuous spaces. *J Global Optim* 11:341–359
- Sukeshwala RN, Sethna SF (1969) Layered gabbro of composite plug of Phenaimata, Gujarat State. *J Geol Soc India* 10:177–187
- Sultan AS, Mansour SA, Santos FM, Helaly AS (2009) Geophysical exploration for gold and associated minerals, case study: Wadi El Beida area, South Eastern Desert. *Egypt J Geophys Eng* 6:345–356
- Tamanyu S (1985) Stratigraphy and geological structures of the Hoho geothermal area, based mainly on borehole data. *Reports Geol Surv Japan* 264:115–142 ((in Japanese))
- Telford WM, Geldart LP, Sheriff RE (1990) Applied geophysics, 2nd edn. Cambridge University Press, Cambridge
- Tlas M, Asfahani J (2018) Interpretation of gravity anomalies due to simple geometric- shaped structures based on quadratic curve regression. *Contrib Geophys Geod* 48:161–178
- Uzun S, Erkan K, Jekeli C (2020) Using gravity gradients to estimate fault parameters in the Wichita Uplift region. *Geophys J Int* 222:1704–1716
- Yang X-S (2013) Bat algorithm: literature review and applications. *Int J Bio-Inspir Com* 5:141–149
- Yang X-S (2010) A new metaheuristic bat-inspired algorithm, in: Gonzalez J, Pelta D, Cruz C et al (Eds.), Nature Inspired Cooperative Strategies. Springer, Berlin, pp: 65–74
- Zhang J, Zhong B, Zhou X, Dai Y (2001) Gravity anomalies of 2D bodies with variable density contrast. *Geophysics* 66:809–813
- Zhang P, Yu C, Zeng X, Tan S, Lu C (2022) Ore-controlling structures of sandstone-hosted uranium deposit in the southwestern Ordos Basin: Revealed from seismic and gravity data. *Ore Geol Rev* 140:104590

